Synthesis and application of nano-hematite on the removal of carcinogenic textile remazol red dye from aqueous solution

Shaimaa M. Ibrahim*, Mona A. Naghmash, Sahar A. El-Molla

Chemistry Department, Faculty of Education, Ain Shams University, Cairo, Egypt, Fax: +20-23370931; emails: shimaaabdelaal@edu.asu.edu.eg (S.M. Ibrahim), Mona_ali@edu.asu.edu.eg (M.A. Naghmash), saharelmolla@edu.asu.edu.eg (S.A. El-Molla)

ABSTRACT

Four nano-hematite adsorbents (α-Fe$_2$O$_3$:Fe-P-T, Fe-W-3w, Fe-W-3d, Fe-A-3) were prepared via precipitation and/or dispersion–precipitation methods. The prepared adsorbents were characterized by X-ray diffraction, Fourier transforms infrared, high-resolution transmission electron microscopy and specific surface area analysis. These newly prepared adsorbents were applied for the removal of Remazol Red (RB-133) dye from aqueous solutions. Fe-W-3w adsorbent showed superior dye removal efficiency (100%), which may be attributed to its small crystal size and high surface area. Pseudo-second order and Langmuir equations describe perfectly the adsorption kinetics and isotherms for the investigated system. The factors affecting Remazol Red (RB-133) adsorption mechanism are discussed.

Keywords: Nano-hematite; Dispersion–precipitation method; Adsorption; Remazol Red (RB-133)

1. Introduction

It is well-known that iron oxide naturally exists in three forms: magnetite (Fe$_3$O$_4$), maghemite (γ-Fe$_2$O$_3$) and hematite (α-Fe$_2$O$_3$) [1]. Hematite is the most stable phase, inexpensive and non-hazardous. Besides these environmental properties, hematite has useful magnetic properties [2]. Hematite has been used broadly in many fields such as environmental protection, Li-ion batteries, water splitting, catalysis and biomedical applications [2]. Furthermore, nano-iron oxide is a promising material for wastewater treatment because of its high surface area and paramagnetic properties [3]. There are many methods applied in the field of removal of dyes and heavy metals such as physico-chemical, coagulation–flocculation, biological, membrane and adsorption processes. In general, the adsorption process is the fastest, simplest, cheapest and most effective technique adopted widely in wastewater treatment [4–8]. Dyes adsorption is an effective process to produce high-quality water via water treatment [9,10]. Synthetic dyes are one of the most important pollutants in the environment which negatively affects the human and aqueous life. Remazol Red (RB-133) is a synthetic dye that is widely used because of its large size and high affinity to bind with cellulosic fiber [11]. It is known that this dye is less reactive than other dyes, therefore, part of this dye remains in dyeing bath or drained off as industrial effluents [12,13]. So, it is very important to apply active adsorbents for removing this carcinogenic dye. In previous studies, adsorbents such as MgO, MgO/Fe$_2$O$_3$, commercial charcoal, activated sawdust and CeO$_2$-Fe$_2$O$_3$-Al$_2$O$_3$ were used for Remazol Red removal [12,14–16]. Up to our knowledge, hematite as an adsorbent for this dye is not used for this purpose till now. Even we thought it may be a promising adsorbent for Remazole red removal [2,17,18].

Nano-iron oxide can be prepared by different techniques, such as precipitation, sonochemical [19], hydrothermal [20], sol-gel [21] and hydrolysis [22]. The precipitation method is considered a facile method that allows preparing metal oxide, but with a difficulty in controlling the particle size products [23,24]. Dispersion–precipitation technique was used to prevent particle agglomeration during the preparation. In this method, the addition of acetic acid to metal hydroxide solution can break the bulk hydroxide particles into small ones forming

* Corresponding author.

colloidal dispersions. Thence the addition of the precipitating agent leads to the desired nanosized product [25,26].

This investigation aims to synthesize and analyze the properties and morphologies of the prepared nanosized iron oxide (hematite) via a facile environmental dispersion–precipitation method. Furthermore, the ability to use these nanoparticles to adsorb the carcinogenic textile pollutant dye, Remazol Red (RB-133) (its structure shown in Fig. 1), is also investigated. The effects of different parameters such as preparation conditions, solution reaction temperature, pH, initial concentrations and contact time are examined in batch mode. Also, the adsorption kinetics, isotherms, thermodynamic parameters and reusing are studied.

2. Experimental

2.1. Materials

Iron nitrate nonahydrate, ammonium hydroxide (28 vol.%), acetone, glacial acetic acid, Remazol red (RB-133), sodium hydroxide and hydrochloric acid were purchased from Sinopharm Chemical Reagent Company Limited. All reagents were of analytical grade and used as received. Distilled water was used in all preparations.

2.2. Synthesis of nanosized iron oxide

Nano-iron oxide was prepared by various techniques and the samples were nominated as follows: (i) Fe-P-3, this sample was prepared by traditional precipitation method from ferric nitrate solution using 1 M NH_4OH solution at pH = 8, temperature 80°C and stirring for 2 h. Then, the carefully washed precipitate was dried at 110°C till constant weight, finally calcined in a muffle furnace at 300°C for 3 h. (ii) The samples prepared by the previous traditional precipitation method and calcined at 400°C and 500°C were nominated as Fe-P-4 and Fe-P-5, respectively. (iii) Fe-W-3w, colloidal dispersion of hydrous ferric oxide was prepared through a method reported recently called dispersion–precipitation method [25,27,28]. A certain amount of iron nitrate nonahydrate was dissolved in ultrapure water, then 1 M ammonium hydroxide was added slowly to the solution with continuous stirring to form hydroxide slurry at pH = 8 and temperature 80°C. The hydroxide precipitate was washed and collected. After that, directly 12.2 mL of glacial acetic acid was added to the wet hydroxide precipitate. The resulting slurry was stirred for 2 h until a colloidal dispersion of hydrous ferric oxide was formed. 100 mL of bidistilled water was added to the above colloidal solution and precipitation occurred immediately. The obtained hydroxide was dried at 110°C till constant weight and calcined at 300°C for 3 h.

(iv) Fe-W-3d, after preparing a portion of hydroxide as shown in technique (iii), the obtained iron hydroxide was not initially treated with glacial acetic acid collected by centrifugation and left overnight then heated at 110°C till constant weight, then the dispersion process was applied by using 12.2 mL glacial acetic acid with stirring, and the obtained colloidal solution was precipitated with 100 mL bidistilled water. The obtained precipitate was collected; dried at 110°C till constant weight and calcined at 300°C for 3 h.

In dispersion–precipitation method, water was replaced by acetone for comparison as follows: (v) Fe-A-3, in this sample the dispersion–precipitation process was applied as shown in technique (iii) but instead of water as precipitating agent, 100 mL of acetone was used. The obtained hydroxide was collected by centrifugation and dried at 110°C followed by calcination at 300°C for 3 h.

2.3. Techniques

A Bruker diffractometer (Bruker D 8 advance target) in Metal Research and Development Center, Cairo, Egypt was used to determine the X-ray diffractograms of the as-prepared solids. The patterns were run at 40 kV and 40 mA with second monochromator CuKα (λ = 1.5405 Å). The scanning rate was 8° and 0.8° in 2θ min^{-1} for phase identification and line broadening profile analysis, respectively. The crystallite sizes of the phases present in the prepared samples were determined using the Scherrer equation [29]:

$$d = \frac{K\lambda}{\beta_{1/2}}\cos\theta \qquad (1)$$

where d is the mean crystalline diameter, λ is the X-ray wavelength, K is the Scherrer constant (0.89), $\beta_{1/2}$ is the full width at half maximum of the main diffraction peaks of the crystalline phase present and θ is the diffraction angle.

Fourier transforms infrared (FT-IR) spectra were carried out using a Shimadzu Prestige-21spectrometer (Chemistry Department, Faculty of Education, Ain Shams University, Egypt) in the range 400–4,000 cm^{-1}, using KBr pellets and resolution of 4 cm^{-1}.

The prepared nano-iron oxide structure and surface morphology in the prepared samples were examined using the (HR-TEM) microanalysis system (JEM-2100CX [JEOL]).

The surface properties of the samples were evaluated by physical adsorption of nitrogen gas at −196°C using a Quantachrome NOVA 2000 automated gas-sorption apparatus model (Petroleum Research Institute, Cairo, Egypt). The samples were degassed at 200°C for 2 h before each
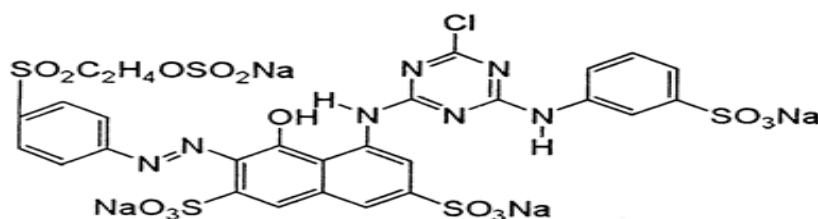
Fig. 1. Remazol Red RB 133 dye molecular structure.

sorption measurement. The specific surface area (S_{BET}) was calculated by applying a Brunauer–Emmett–Teller (BET) equation [30]. The pore size distribution was calculated using the Barrett, Joyner, and Halenda (BJH) method [30].

2.4. Preparation of Remazol Red (RB-133) solution

A stock solution was prepared by dissolving an accurately weighed quantity of the dye in bi-distilled water. The stock solution was used to prepare solutions for adsorption tests by successive dilutions to the desired concentrations. The absorbance was determined by UV–vis spectroscopy. The absorbance data for each experiment were converted into concentrations for kinetic and equilibrium results as reported in previous studies [14,15].

2.5. Kinetic adsorption studies

A series of Remazol Red (RB-133) solution removal experiments using nano ferric oxide as adsorbent was carried out. The effect of contact time was studied to determine the time taken by adsorbents to reach equilibrium at pH = 3 and 7 with initial dye concentrations fixed at 50 ppm, 50 mg adsorbent dose and temperature 25°C. The dye concentration was measured at different time intervals up to 3 h. The solution samples were centrifuged after finishing the adsorption experiments, at 7,000 rpm for 15 min. Shimadzu UV/Vis1601 spectrophotometer in Chemistry department, Faculty of Education, Ain Shams University, Egypt was used to measure the concentration of the residual dye at an appropriate wavelength (λ_{max} = 520 nm). This data was used to calculate the adsorption capacity of the adsorbent. A similar procedure was applied as a blank for another set of solutions containing the same dye concentration without adsorbent.

The aqueous samples were taken at present time intervals, and the concentrations of dyes were similarly measured. The adsorption amount at time t, q_t (mg/g) is calculated by [14,15] the following equation:

$$q_t = (C_0 - C_t)\frac{V}{W} \tag{2}$$

where C_0 and C_t (mg/L) are the concentrations of dye at beginning and time t, respectively; V is the volume of the solution (L); W is the mass of dry adsorbent used (g). Effect of dye adsorption temperature was carried out for 3 h at (25°C, 35°C and 45°C) at pH 7.0 using 50 mg adsorbent and initial dye concentration equal 50 ppm.

2.6. Equilibrium adsorption studies

Langmuir and Freundlich isotherm models were employed to investigate the adsorption process and to do this, 100 mL of dye solutions with different initial dye concentrations (10–100 ppm) were prepared. Each dye solution was shaken with (50 mg) of the adsorbent and the mixture was then kept at (25°C ± 0.1°C, and pH = 7) for 3 h to reach equilibrium. The amount of adsorption at equilibrium time t, q_e (mg/g) is calculated by

$$q_e = (C_0 - C_e)\times\frac{V}{W} \tag{3}$$

where C_0 and C_e (mg/L) are the concentrations of dye at t = 0 min and at equilibrium time, respectively; V is the volume of dye solution (L); W is the mass of dry adsorbent used (50 mg).

2.7. Effect of pH

The pH of the dye solution is an important parameter that affects the adsorption performance of dye molecules. In this study, initial dye concentrations = 50 ppm in the pH range of 3–11 (using 0.1 M HCl and NaOH) were adjusted and measured by (pH meter OHAUS-STARTER 3000). Then 50 mg of adsorbent was added for each solution and the solution was shaken for 3 h (150 rpm at 25°C). Then, centrifugation of the solution at 7,000 rpm for 15 min was applied. Finally, the solutions were analyzed with UV/vis spectrophotometer and the removal percentage of dye (R%) was calculated by Eq. (4):

$$\%R = \frac{C_0 - C_t}{C_0}\times 100 \tag{4}$$

where C_0 is the initial dye concentration and C_t is the dye concentration at time (t).

2.8. Adsorbent reusing

To investigate the efficiency of the prepared samples and how many times can be used as an adsorbent, the following experiments were performed. The adsorbent samples were used four times successfully and after each experiment, the adsorbent was washed with NaOH solution (0.01 M) for 2 h and then reused. This step was repeated before each reusing experiment.

3. Results and discussion

3.1. X-ray diffraction analysis

Fig. 2 shows the X-ray diffraction (XRD) patterns of various Fe-prepared samples. It illustrates peaks at 2θ values of 24.16°, 33.12°, 35.63°, 40.64°, 49.47°, 54.08° and 57.42° attributed to Fe_2O_3 (JCPDS Card Number of 33-0664), the peaks can be attributed to the 012, 104, 110, 113, 024, 116 and 018 crystalline structures which confirm the hematite phase
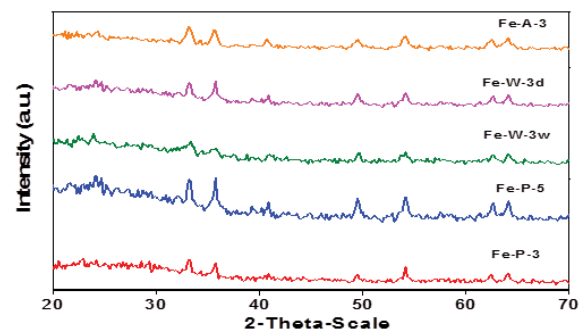
Fig. 2. XRD patterns of Fe_2O_3 precipitations performed at different conditions.

Table 1
Effect of preparation condition and calcination temperature on the crystallite size of precipitated Fe_2O_3 system

Sample	Calcination temperature (°C)	Crystal size (nm)
Fe-P- T	300	17.98
Fe-P- T	500	38.49
Fe-W-3w	300	3.00
Fe-W-3d	300	17.50
Fe-A-3	300	15.06

Fig. 3. FTIR spectra of different Fe_2O_3 precipitations calcined at 300°C.

for Fe_2O_3 [31]. The diffraction lines are broad and weak, signifying its low crystallinity and small particle size [32]. The crystal size was estimated by Scherrer's equation [33]. We can conclude from the results obtained the following: (i) By increasing calcination temperature of Fe_2O_3 sample prepared by traditional precipitation method from 300°C to 500°C, no change in peaks location was observed but the peak intensity and the crystal size increased as shown in Table 1. This result suggests that the crystal's growth is directly proportional to the calcination temperature [34]. (ii) Also, It was clear that the dispersion precipitation for sample Fe-W-3w resulted in a decrease in the particle size comparing with normal precipitation method Fe-P-3 as shown in Table 1. This decrease attained sixfold. It seems that the acetic acid addition to the wet iron hydroxide and using water as precipitating agent converted the bulk hydroxide to small particles, forming a colloidal dispersion [26], which affected the crystalline structure of the calcined sample at 300°C. (iii) Applying dispersion precipitation process for dried iron hydroxide and using water as precipitating agent for Fe-W-3d did not change the particle size in comparison with traditional precipitation Fe-P-3 as shown in Table 1. (iv) Also, it is clear from Fig. 2 and Table 1 that using water Fe-W-3w decreases the particle size more than acetone Fe-A-3. This result emphasizes the effect of using water as a precipitating agent, which can weaken the colloidal dispersions including hydrous iron oxide forming precipitates of metal oxides with smaller particle sizes [25].

3.2. FT-IR

Infrared spectroscopy has been used to determine the surface functional groups of synthetic Fe_2O_3. Fig. 3 demonstrates the FTIR spectra of Fe_2O_3 samples in the range of 400–4,000 cm^{-1}. The observed broadband at 3,420 cm^{-1} assigned to stretching vibrations of H_2O molecules [35], but the band at 1,633 cm^{-1} is corresponding to the bending vibrations of H_2O molecules [36]. The IR spectrum shows two peaks located at around 538, 440 cm^{-1}, which confirms the presence of Fe–O vibrations mode of hematite [37]. The other small band at 1,380 cm^{-1} was attributed to the Fe–O stretching vibration, which proved the growth of pure hematite phase [38]. The presence of the α-Fe_2O_3 (hematite) phase in all prepared samples calcined at 300°C, detected by XRD was confirmed by the IR bands. The small absorption bands at about 2,923 cm^{-1} could be due to the hydrocarbon impurities [39].
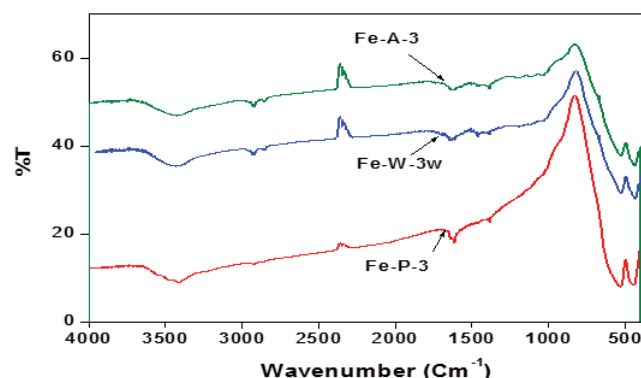
3.3. HR-TEM analysis

Fig. 4 illustrates the HR-TEM images of Fe_2O_3 samples prepared by precipitation Fe-P-3 and by dispersion–precipitation Fe-W-3w. It can be noticed that the particles of all applied solids have uniform spherical shapes with agglomeration, with average particle size 17.42 and 11.84 nm, respectively. From these results, using the solvents dispersion method decreases the agglomeration of particles which leads to the formation of solids with small particle sizes.

3.4. Nitrogen adsorption–desorption analysis

Nitrogen adsorption–desorption isotherms technique was carried out to describe the porous structure and the BET surface area of the prepared nano-iron oxide samples as shown in Fig. 5a. The pore-size distributions of the investigated solids are shown in Fig. 5b. Table 2 includes the values of the BET surface area, pore volume and pore diameter of the synthesized solids. Inspecting Figs. 5a, b and Table 2, we noticed that: (i) all isotherms are of Type IV with H3-type hysteresis loops signified that all hematite samples are slit-shaped mesoporous [40,41]. (ii) Fig. 5b showed a narrow pore size distribution with an average pore diameter located between 5.41 and 10.68 nm. (iii) Table 2 shows that the Fe_2O_3 sample (Fe-P-3) possesses S_{BET} value (43.38 m^2/g), which decreases with increasing the calcination temperature to 500°C. Increasing the calcination temperature decreases both the surface area and the pore volume values as a result of crystal growing and particle aggregation [42]. (iv) Fe-samples prepared by the dispersion and precipitation method have bigger S_{BET} values than that prepared by traditional precipitation. This may be due to the role of glacial acetic acid as a dispersing agent which prevents Fe-nanoparticles agglomeration [43,44]. (v) Using excess of water as precipitating agent increased the S_{BET} and pore volume as shown in Table 2 for Fe-W-3w, Fe-W-3d more than Fe-A-3 sample in which acetone is used as a precipitating agent. This may be due to water adsorption on the surface of the outer nanoparticles which enhanced the formation of hydroxide surface layer. Also, the possible extraction of acetic acid molecules from Fe nanoparticles surface by water molecules affected the precipitate stability and was followed by an observed decrease in the particle size and increase in the BET surface area of the synthesized solids.
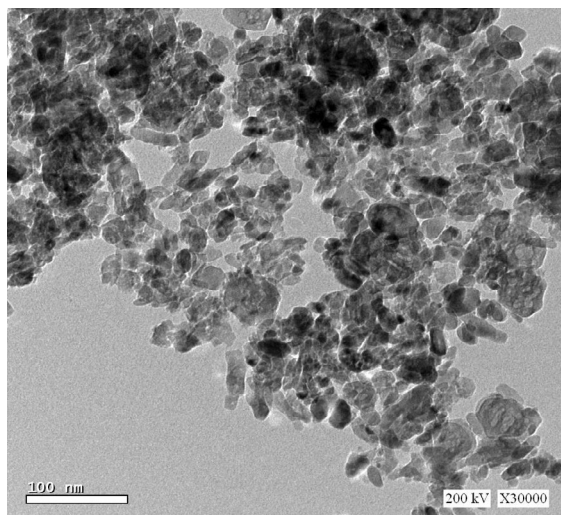
Fe-P - 3
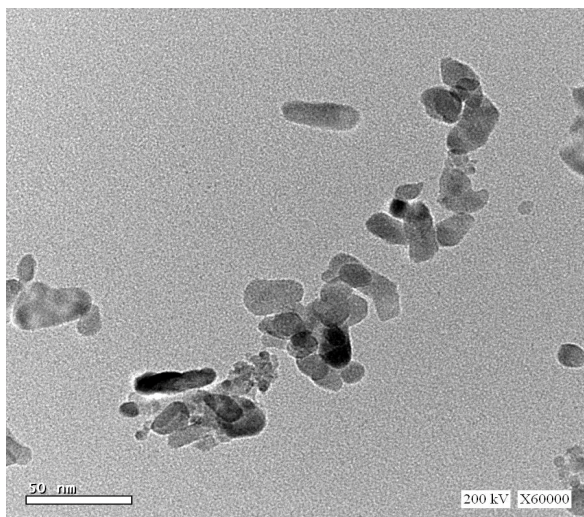
Fe-W-3w

Fig. 4. High resolution transmission electron microscopy (HRTEM) images for Fe-samples calcined at 300°C.

3.5. Adsorption experiments

The effects of preparation conditions of the adsorbents on the adsorption parameters have been studied. Also, many variables affecting the dye adsorption as contact time, temperature, initial concentration and pH of Remazol red (RB-133) dye solution will be discussed.

3.5.1. Effect of various preparation conditions

3.5.1.1. Effect of calcination temperature

Batch adsorption of Remazol red (RB-133) on the Fe-P-T adsorbent calcined at 300°C, 400°C, 500°C was studied at initial dye concentration 50 ppm, pH = 7, temperature 25°C and an adsorbent dose of 50 mg. The results obtained were

plotted in Fig. 6. Inspection of Fig. 6: (i) the dye removal reaches equilibrium at 60 min on calcined Fe-P-T samples. (ii) The removal efficiency of the dye by Fe-P-3 was (>62%) higher than the other calcined solids. This may be due to the small crystallite size of the Fe_2O_3 phase (c.f. XRD results from Table 1) which attained 17.9 nm in Fe-P-3 samples. The observed decrease in % of dye removal as a result of increasing the calcination temperature from 300°C to 500°C could be attributed to a significant increase in the adsorbent crystal size (Table 1), and a decrease in its S_{BET}, besides the observed pore widening (Table 2). These effects decrease the surface affinity to Remazol red (RB-133) and limit the adsorption percentage. (iii) It seems that Fe-P-4 and Fe-P-5 have the same behavior towards lower dye removal. So, the sample calcined at 300°C Fe-P-3 is the most efficient adsorbent for dye uptake.

3.5.1.2. Effect of precipitation method modifiers

It was reported that dissolving ferric hydroxide in glacial acetic acid led to obtaining the reddish-brown solution as the same as of the partially hydrolyzed ferric (III) solution promoted by alkali [27]. Also, the weak acid such as acetic acid cannot break thoroughly all the Fe–O bonds in the hydroxides to form simple ferric ions [28] but could be adsorbed over particles surface via strong carboxyl group interactions [45,46]. It seems that acetic acid molecules act as ligands or as stabilizing agents and prevent the ferric precursor aggregation [27]. The effect of the precipitating agent for highly dispersed nano-sized species has been investigated. Using water as a precipitating agent for nanosized manganese hydroxide dispersed in acetic acid solution was reported [27,47]. Acetone also was used as a precipitating agent for hydrous ferric oxide from colloidal solutions [25]. However, in the present work, the effect of using the two different precipitating agents through dispersion–precipitation method on the efficiency of the adsorbent towards Remazol red (RB-133) dye removal was well studied.

The % of dye removal over the nominated samples Fe-P-3, Fe-W-3w and Fe-A-3 is shown in Figs. 7a–c. In Figs. 7a and b it is clear that: (i) the % of dye removal increased progressively with time and attained equilibrium with 100% and 80% in presence of Fe-W-3w and Fe-P-3 adsorbents through 180 min, respectively (upon dye concentration = 25 ppm, pH = 3, 25°C). The biggest removal % observed in the case of the Fe-W-3w sample may be related to its high surface area as shown in Table 2 (62.71 m²/g), or the small crystallite size (as shown in XRD and TEM sections). The small crystallite size of the Fe-W-3w sample may refer to the preparation technique in which, the partial dissolution process of the ferric hydroxide in glacial acetic acid solution caused fracture into small particles of hydrated Fe_2O_3 form and using water as precipitating agent causes further decrease in the crystal size of ferric species. (ii) The % removal of Remazol red (RB-133) dye in the presence of the Fe-A-3 sample attained equilibrium with only 64% at contact time 180 min (Fig. 7b). This behavior can be attributed to the observed increase in its crystallite size which is followed by a decrease in its surface area 53.71 m²/g (Table 2).

Effect of using the wet (Fe-W-3w) or dried (Fe-W-3d) iron hydroxide precipitates before acetic acid treatment was investigated as shown in Fig. 7c. It is clear that (i) Fe-W-3w
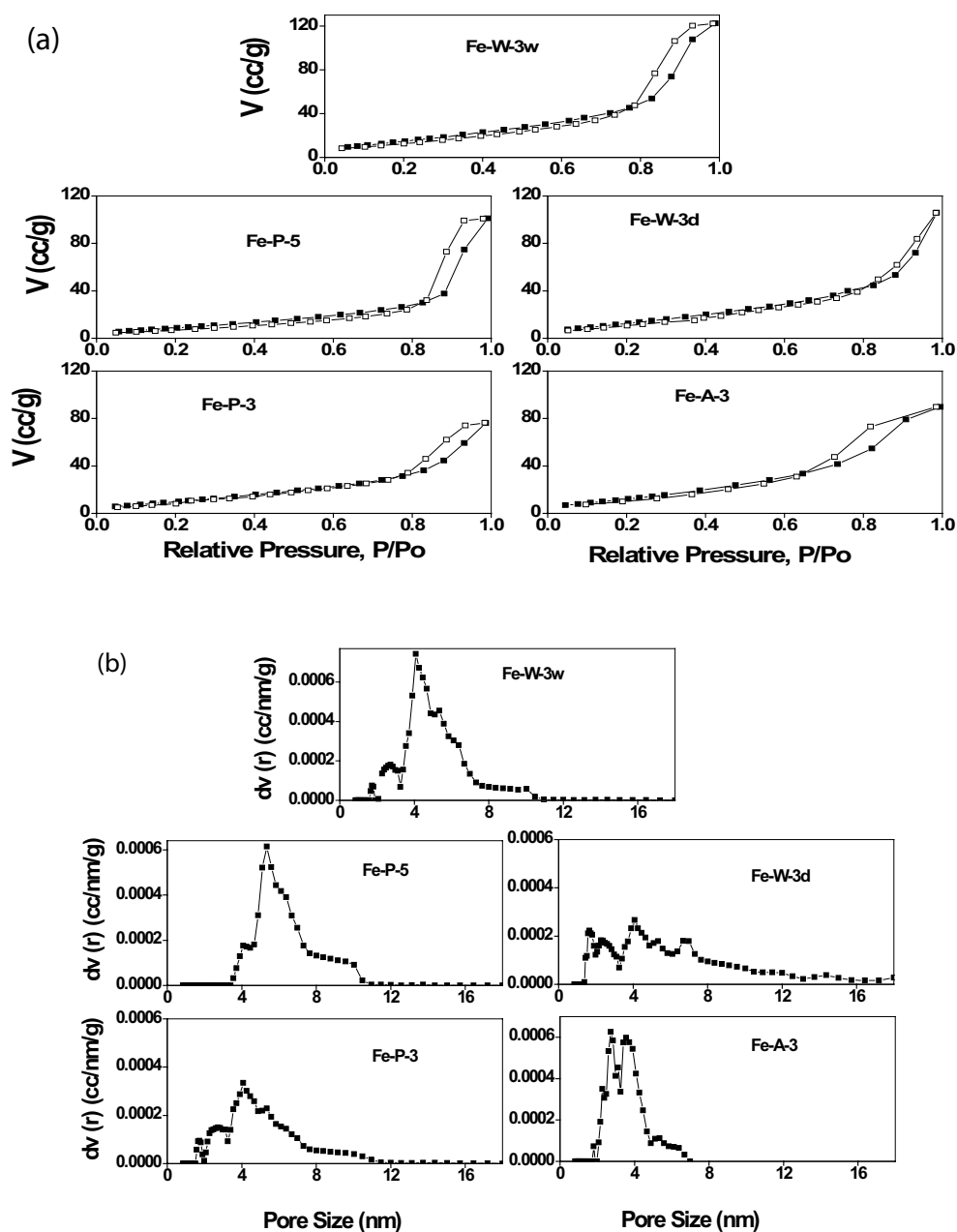
Fig. 5. (a) Representative isotherms for the prepared samples according to different recipes. (b) The pore size distribution for the prepared samples according to different recipes.

Table 2
Surface characteristics of solids derived from different recipes after calcination at various temperatures

Catalyst	Calcination temperature (°C)	S_{BET} (m²/g)	V_P (cm³/g)[a]	Pore diameter (nm)[b]
Fe-P- T	300	43.38	0.152	8.15
Fe-P- T	500	37.23	0.114	10.68
Fe-W-3w	300	62.71	0.184	8.15
Fe-W-3d	300	56.99	0.159	8.15
Fe-A-3	300	53.71	0.135	5.41

[a]Pore volume determined around saturation pressure.
[b]Calculated by BJH method.
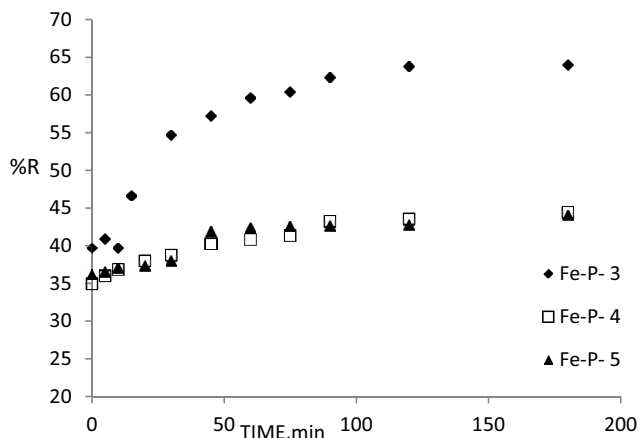
Fig. 6. Effect of calcination temperature on the removal percentage of Remazol Red (RB-133) by Fe-P-T nanomaterial calcined at different temperatures (adsorbent dose = 50 mg), (dye concentration = 50 ppm, at 25°C and at pH = 7).

acts as an efficient adsorbent more than Fe-W-3d. (ii) Fe-W-3d is more efficient than Fe-P-3, where the % removal attained 90% and 80%, at contact time 180 min, respectively (at adsorption conditions pH = 3, dye concentration = 25 ppm, 25°C). The above behavior can be explained in terms of the crystallite size of hematite and also the specific surface area of the prepared adsorbents. (iii) The adsorbents efficiency towards dye removal increases as in the following order: Fe-W-3w > Fe-W-3d > Fe-P-3 > Fe-A-3. This finding indicates clearly that dispersion and precipitation process for wet iron hydroxide followed by calcination at 300°C accelerates the formation of nano-sized particles of the Hematite phase for Fe_2O_3 and/or increases its surface area (Table 2), these parameters enhance the dye removal. These results indicate that the synthesized nano-hematite nominated as Fe-W-3w is a promising adsorbent for dyes removal from aqueous solutions.

3.5.2. Effect of contact time and solution temperature on Remazol red (RB-133) removal

Figs. 7a–c show the variation of % of Remazol Red (RB-133) as a result of using Fe-P-3, Fe-W-3w and Fe-A-3 adsorbents as a function of time, which indicates that the rate of adsorption by iron oxide nano-spheres at the initial time is high and increases by increasing contacting time within 30 min. Vacant adsorption sites on adsorbent material may be occupied by dyes deposited and maximum removal was attained till 180 min. So, the optimum contact time will be 180 min for all experiments.

Because of the vital effect of temperature on the adsorption process as it can increase or decrease the amount of adsorption, this factor has been studied. The adsorption of Remazol red (RB-133) was achieved at three temperatures (at 25°C, 35°C and 45°C) onto Fe-P-3 as shown in Fig. 8. The results discovered that the dye uptake % increased with increasing temperature from 25°C to 45°C. This suggests that the adsorption is an endothermic process and the higher temperature is more proper for the dye adsorption. The observed increase in the adsorption may be due to the increase in dye
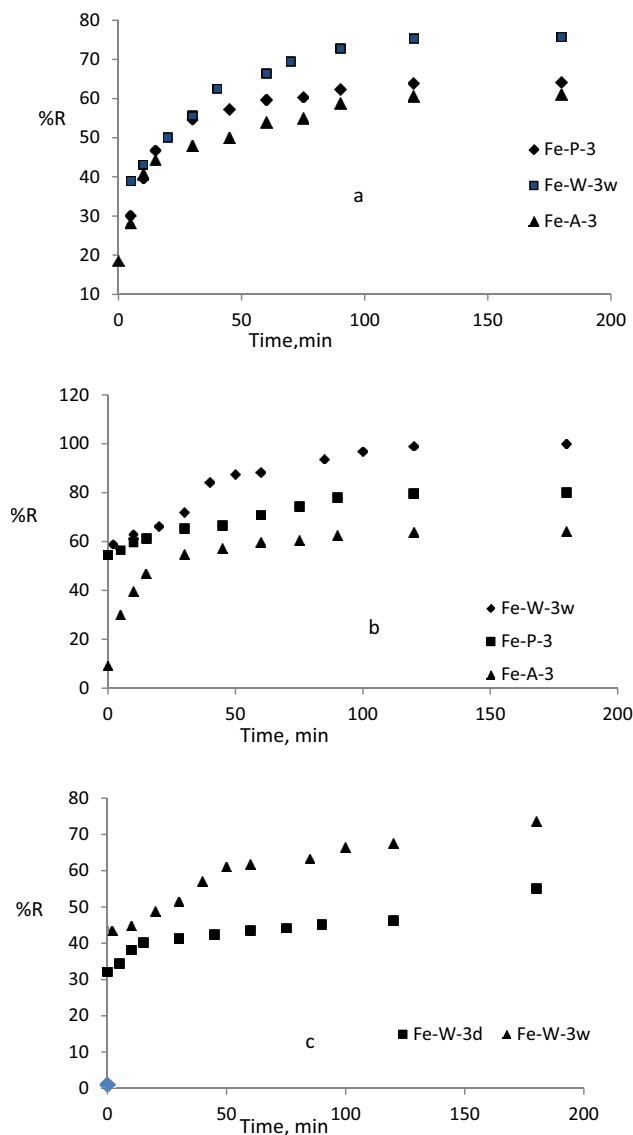
Fig. 7. Effect of preparation condition and time of contact on the % of Remazol Red (RB-133) removal by different prepared nanomaterials at 25°C (adsorbent dose = 50 mg), (a) (dye concentration = 50 ppm, and at pH = 7), (b) (dye concentration = 25ppm, and at pH = 3) (c) (dye concentration = 25 ppm, and at pH = 7).

molecules' mobility with temperature. It is known that rising temperature increases the diffusion rate of the adsorbed molecules through the external boundary layer and the internal pores of the adsorbent particles, because of decreasing the solution viscosity [48,49] and increasing the adsorption ready active sites [50].

3.5.3. Effect of initial dye concentration

The Remazol red (RB-133) uptake was examined at initial concentrations 10, 25, 50 and 100 ppm for the investigated adsorbents as shown in Figs. 9a and b. The % of adsorption decreases with increasing dye concentration in the solution (>50 ppm). This observation may be due to the fullness of
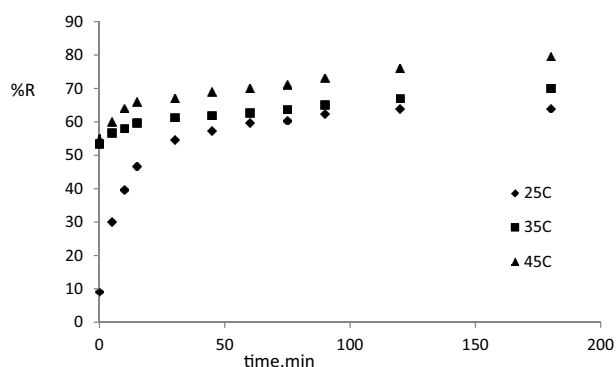
Fig. 8. Effect of temperature on the removal percentage of Remazol Red (RB-133) over Fe-P-3, at pH = 7, dye concentration = 50 ppm, adsorbent dose = 50 mg.

adsorption sites on the adsorbent surface with dye molecules. The same behavior was observed in the literature for the removal of RB5 by iron oxide CNPs [3]. Also, Zhang et al. [51] found that when the Methyl Orange concentration increased from 20 to 400 mg/L, the percentage of dye uptake by chitosan/alumina interface decreased from 99.53% to 83.55%. Plus, Jarusiripot [52] found that the adsorption% of Remazol Brilliant Blue R by bottom ash pretreated with HCl was 90% at low dye concentrations and about 50% at higher dye concentration. However, in all adsorption experiments for different nanomaterials, the initial dye concentration will be constant at 25 or 50 ppm.

3.5.4. Effect of solution pH

The performance of adsorption in wastewater treatment is mostly influenced by the solution pH. This is because of the change in pH results in variation in the degree of the adsorptive molecule ionization and the adsorbent surface characteristics [53]. The effect of solution pH was assessed in the range from 3 to 11.0 (adjustment occurred with 0.1 M HCl or 0.1 M NaOH) at a constant temperature of 25°C and 25 ppm initial dye concentration in the presence of Fe-W-3w adsorbent calcined at 300°C (Fig. 9c). Inspection of Fig. 9c, % of dye removal decreases with increasing solution pH, the maximum dye removal in presence of Fe-W-3w solid was 100% ratio at pH = 3, while at pH = 11 the maximum adsorption % decreased to 48.3%. This behavior indicates that the removal % of Remazol red (RB-133) was higher at the acidic conditions. This result can be explained by studying the structure of the dye and adsorbent point of zero charges (pH$_{pzc}$). The increase in the pH of the system leads to decreasing the number of (+) charged sites and increasing the number of (−) charged sites [15]. The adsorption of the anionic dye is more favorable on the adsorbent positively charged surface sites (at pH < pH$_{pzc}$) with electrostatic attraction [14,54]. It has been reported that pH$_{pzc}$ of hematite (α-Fe$_2$O$_3$) is 7.8 [55,56] and according to the following equations: at pH < (pH$_{pzc}$ = 7.8) the adsorbent surface (MOH) will be covered by H$^+$ ions and MOH$_2^+$ will be obtained. But, at pH > (pH$_{pzc}$ = 7.8) OH$^-$ reacts with the (MOH) to give (MO$^-$).
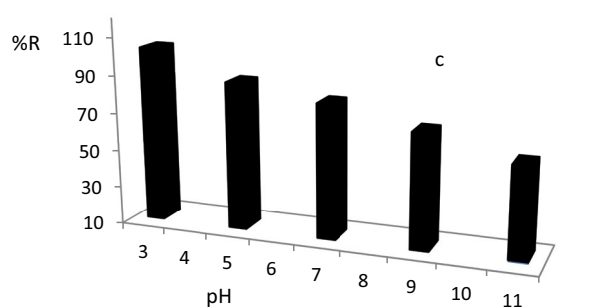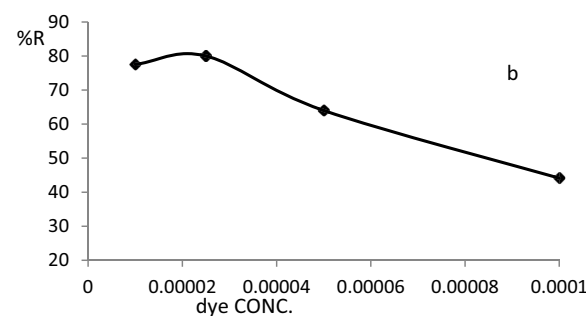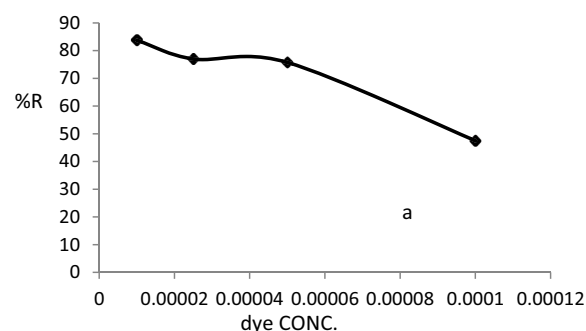
Fig. 9. Effect of dye concentration on the removal percentage of Remazol Red (RB-133) at 25°C, pH = 7 (adsorbent dose = 50 mg) after 3 h over (a) Fe-W-3w, (b) Fe-P-3, and (c) effect of solution pH by Fe-W-3w nanomaterial (dye conc. = 25 ppm, at 25°C, adsorbent dose = 50 mg, after 3 h).

$$MOH + H^+ \rightarrow MOH_2^+$$
$$MOH + OH^- \rightarrow MO^- + H_2O$$
$$MOH_2^+ + 2OH^- \rightarrow MO^- + 2H_2O$$
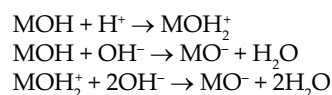
At pH range from 3 to 7, a significant altitude electrostatic attraction dwells between the positively charged surface of the adsorbent and anionic dye, so the high removal percentage was obtained. The contrast, at pH (9–11) repulsion forces present between anionic Remazol red (RB-133) dye and negative surface charge led to a decrease in the removal efficiency. Therefore, the best pH for higher removal from aqueous solution is between 3 and 7. The same behavior is also reported in previous studies for the adsorption of different dyes over different adsorbents [48,57,58].

To elucidate the efficiency of the prepared samples in the dye adsorption, a comparison of the maximum dye removal percentage over the as-prepared iron adsorbents in this work with other iron adsorbents previously reported in

the literature is shown in Table 3 [3,50,59–64]. Inspection of Table 3, it can be observed that the maximum removal % and high adsorption capacity of Remazol red (RB-133) dye onto Fe-W-3w adsorbent (100%) is achieved and on the top of all removal percentages of the anionic or cationic dyes reported in the literature for other iron oxide adsorbents.

Finally, we can say in this study that an environmental friendly nano-Fe-W-3w adsorbent was prepared via dispersion–precipitation method could efficiently adsorb Remazol Red (RB-133) dye with % removal values reached to 100%. So, this synthesized nano-sample was shown to be a very good and cheap adsorbent for the dye removal from aqueous solutions and this is useful in some practical applications.

3.5.5. Adsorption kinetics

The adsorption mechanism of Remazol red (RB-133) by the prepared nanosphere iron oxide was achieved through applying the pseudo-first-order (PFO), and pseudo-second-order (PSO) to fit the experimental data [14,65,66].

The nonlinear equation of pseudo-first-order was represented by:

$$q_t = q_e \left(1 - e^{-k_1 t}\right) \tag{5}$$

where q_t is the amount of dye adsorbed at time t (min), q_e denotes the amount adsorbed at equilibrium, and k_1 (min^{-1}) is the pseudo-first-order adsorption rate constant.

The nonlinear equation of pseudo-second-order can be expressed as the following:

$$q_t = \frac{q_e^2 k_2 t}{(1 + k_2 q_e t)} \tag{6}$$

where k_2 (g/(mg min)) is the adsorption rate constant of pseudo-second-order. The calculated values of k_1 and k_2 are represented in Table 4.

Table 3
Comparison of removal adsorption of different dyes over iron adsorbents

No	Adsorbent	Dye	% of removal	$q_{m'}$ mg/g	Adsorption condition	Kinetic model	Isotherm model	Adsorption enthalpy $\Delta H°$ kJ/mol	Reg. cycles	Reference
1	Magnetic iron oxide	Reactive Yellow	75	25	pH = 7 temp. = 25°C, Ads. dose = 5 mg	FL-PFO	Langmuir–Freundlich	N/A	3	[59]
2	Hollow Zn-Fe$_2$O$_4$ nanospheres	Congo red	–	16.58	pH = 6 temp. = 25°C, Ads. dose = 0.02 g	N/A	Langmuir	N/A	N/A	[60]
3	MgFe$_2$O$_4$	Methylene Blue	57	50	Room temp. Ads.dose = 1 mg/mL	N/A	N/A	N/A	N/A	[61]
4	ZnOeZnFe$_2$O$_4$-PPy	Congo red	78	–	pH = 7 temp. = 25°C, Ads. dose = 0.5 g/L	PSO	N/A	N/A	N/A	[62]
5	Iron oxide	Reactive Black 5	90	11.29	pH = 2, remp. = 25°C, dose = 6 g/L	N/A	Langmuir and Freundlich	24.14	10	[3]
6	Iron-manganese oxide coated kaolinite	Basic fuchsine (BF)	94.5	10.36	pH = 9, temp. = 30°C, dose = 3 g/L	PSO	Langmuir and Toth	6.68	N/A	[50]
7	Halloysite-magnetite-based composite	Methyl violet 2 B	94.7	20.04	pH = 4.2, temp. = 25°C, dose = 0.25 g	PSO	Langmuir	–13.23	4	[63]
8	Iron-manganese oxide coated kaolinite	Crystal violet (CV)	94.8	20.64	pH = 8, Temp. = 30°C, dose = 2 g/L	PSO	Langmuir and Toth	6.7	N/A	[50]
9	Graphene oxide nanocomposites (GO-Fe$_3$O$_4$)	Chrysoidine Y	96	344.83	pH = 7, temp. = 20°C, dose = 5 mg	PSO	Langmuir	–8.19	5	[64]
10	Fe-W-3w	Remazol red(RB-133)	100	64.10	pH = 3, temp. = 25°C dose = 50 mg	PSO	Langmuir	24.5	4	Present study

*N/A: Not applied.

Table 4
Kinetic model constants and correlation coefficients for adsorption of Remazol Red (RB-133) dye onto different samples

Solid	$q_{e,exp}$ (mg/g)	Pseudo-first order model					Pseudo-second order model					Intra-particle diffusion	
		$q_{e,cal.}$ (mg/g)	k_1 (min^{-1})	R^2	%S.D.	χ^2	$q_{e,cal.}$ (mg/g)	k_2 (g/mg min)	R^2	%S.D.	χ^2	k_{dif1} (mg/min$^{1/2}$g)	k_{dif2} (mg/min$^{1/2}$g)
Fe-W-3w	38.7	35.4100	0.0830	0.9507	1.00751	5.6698	39.3270	0.00290	0.9829	0.8907	1.9673	12.4720	0.64594
Fe-P-3	31	29.5400	0.1040	0.9676	0.6373	2.5508	31.457	0.00408	0.9826	0.6725	1.3705	10.8000	0.3514
Fe-A-3	29.4	26.4968	0.11434	0.9449	0.7103	3.2561	28.8267	0.00579	0.9791	0.63215	1.2961	9.8941	0.3752
Fe-P-4	21.5	20.110	0.1949	0.9392	0.5769	1.8063	21.2983	0.01499	0.9597	0.4864	1.43514	–	–
Fe-P-5	21.22	20.322	0.2019	0.9338	0.5555	1.8244	21.3275	0.01538	0.9583	0.4871	1.3773	–	–

The data of adsorption kinetic of Remazol Red (RB-133) by different prepared nanomaterials were analyzed by PFO and PSO kinetic models and plotted in Figs. 10a–c. The result of the fitting, Adj.R^2, standard deviation (S.D.%), and the chi-square factor (χ^2) are listed in Table 4. From the table, it is clear that the (PSO) kinetic model gave high correlation coefficient values ($[R^2] > 0.95$) and low S.D.% for the adsorption of Remazol red (RB-133) dye onto the nano solids; therefore, the best model for kinetics of adsorption Remazol red (RB-133) dye by hematite samples is pseudo-second-order kinetic model. These results suggest that the rate-limiting step may be chemisorption [14,15,67].

Inspecting Table 4, it is obvious that the value of experimental equilibrium adsorption capacity is adjacent to the calculated one (q_e) in case of pseudo-second-order reaction more than that depicted from the pseudo-first-order kinetic model. So, as mentioned before the adsorption kinetics of Remazol Red (RB-133) on different hematite (α-Fe$_2$O$_3$) nanomaterials can be described by pseudo-second-order equation. The applying (PSO) kinetic model suggests the possibility of adsorption of one dye molecule onto two active sites [46].

The intra-particle diffusion probability was detected by utilizing the modified Weber and Morris's equation [14,15,68]:

$$q_t = k_{dif}\, t^{0.5} \tag{7}$$

where k_{dif} is the intra-particle diffusion rate constant (mg/(g min$^{1/2}$)). From the plot of q_t vs. $t^{0.5}$, we calculated the values of k_{dif1} and k_{dif2}, respectively.

Fig. 11 shows the plots of q_t vs. $t^{0.5}$ for Remazol Red RB-133 adsorption by different hematite α-Fe$_2$O$_3$ nanomaterials calcined at 300°C. The results obtained showed the presence of a multi-linear plot, which was discussed by occurrence of two steps. The first is the instantaneous using of the available sites on the sorbent surface (phases I, k_{dif1} its diffusion rate constant). The second step might be due to the slower rate of sorbate diffusion from the surface site into the inner pores (phases II, k_{dif2} its diffusion rate constant) [14,15,67]. The values of k_{dif1} and k_{dif2} for Fe-W-3w, Fe-P-3 and Fe-A-3 are shown in Table 4. It seems the plots do not pass the origin point. Therefore, in the adsorption process, the rate-determining step might be the boundary layer (film) diffusion (the surface diffusion process) [14,15].

The relationship between the (PSO) rate constant (k_2) and absolute temperature T (K) can be described by Eq. (8):

$$k_2 = \mathring{A}\, e^{-Ea/RT} \tag{8}$$

where E_a is the Arrhenius activation energy (kJ/mol), $\mathring{A}$ is the Arrhenius factor (g/mg min), and R is the gas constant (8.314 J/mol K).

The calculated activation energy for dye adsorption onto Fe-P-3 was 25.581 kJ/mol attributed to physisorption.

3.5.6. Adsorption isotherms

This study focused on two isotherms models; Freundlich and Langmuir. The Freundlich model supposes a heterogeneous adsorption surface possessing unequally available sites with different energies of adsorption. The validity of
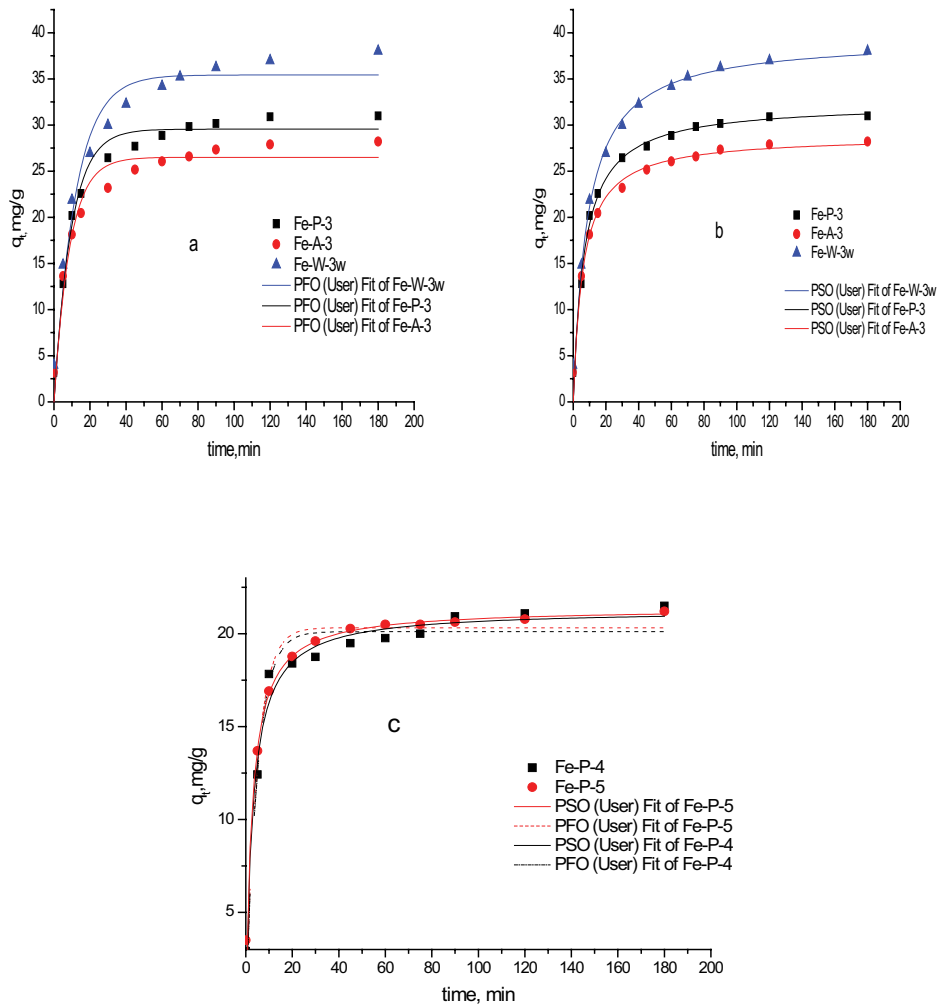
Fig. 10. Nonlinear pseudo-first-order kinetic model (PFO), and nonlinear pseudo second-order kinetic model (PSO), for Remazol Red RB-133 dye adsorption onto different nanomaterial solids calcined at 300°C, 400°C and 500°C (dye concentration = 50 ppm, at 25°C and pH = 7).
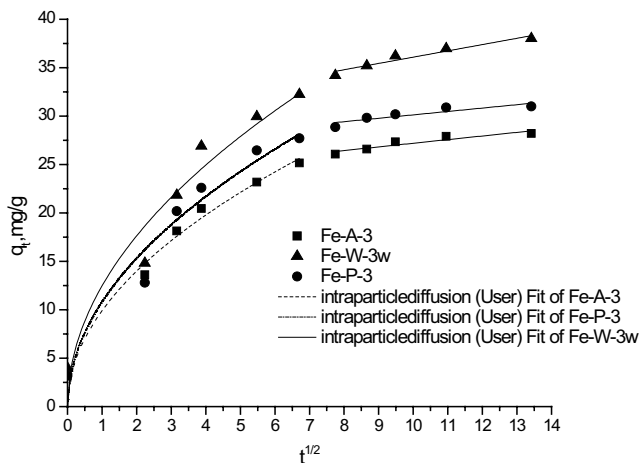
Fig. 11. Intra-particle diffusion model for the adsorption of Remazol red dye onto Fe-W-3w, Fe-P-3 and Fe-A-3.

nonlinear Freundlich adsorption model was established using the following relation [69]:

$$q_e = K_F C_e^{1/n} \tag{9}$$

where K_F and n are Freundlich constants and they are empirical constants that can be related to the adsorption capacity and the adsorption intensity, respectively. When q_e is plotted vs. C_e, the constants K_F and $1/n$ could be calculated from the nonlinear regression.

On the other hand, the Langmuir isotherm model indicates the formation of monolayer coverage of the dye molecule on the outer surface of the adsorbent and demonstrates the homogeneous nature of the sample surface. The nonlinear form of Langmuir isotherm is expressed in Eq. (10) [70]:

$$q_e = \frac{q_{max} \cdot K_L \cdot C_e}{1 + K_L \cdot C_e} \tag{10}$$
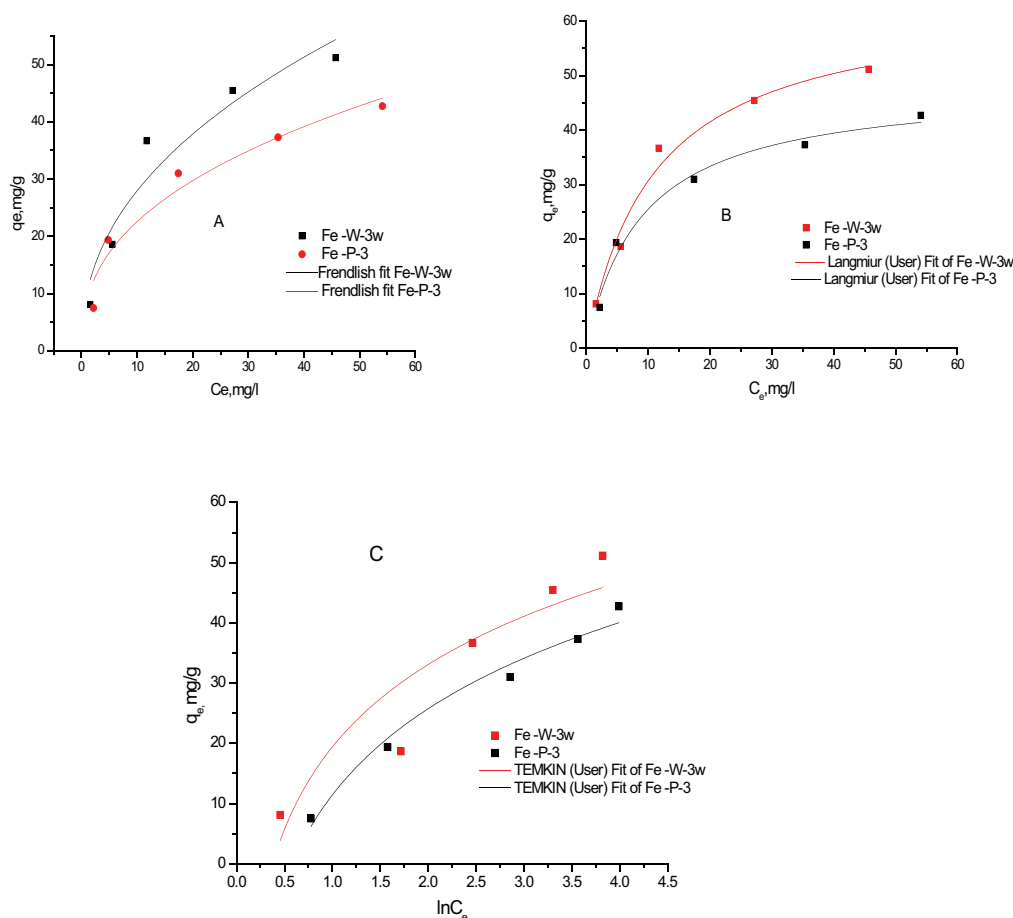
Fig. 12. Nonlinear Freundlich isotherms (a), nonlinear Langmuir isotherms (b), and Temkin isotherms (c) for Remazol Red RB-133 dye adsorption onto Fe-W-3w and Fe-P-3 nanomaterials.

where q_{max} is the monolayer sorption capacity (mg/g) and K_L is Langmuir constant related to the energy of the adsorption (L/mg). The q_{max} and K_L can be obtained from the nonlinear plot of q_e vs. C_e.

Langmuir and Freundlich plots isotherm models on Fe-P-3 and Fe-W-3w are shown in Figs. 12a and b. The results showed that the Langmuir equation yields a curve with a preferable fit of the experimental data than the Freundlich equation over the as-prepared adsorbents. The calculated parameters for the two isotherm models are summarized in Table 5. The Adj. (R^2) of the nonlinear regression plot is ≥0.977 and the very low values for standard error and χ^2 factor by applying Langmuir isotherm model, for both Fe-W-3w and Fe-P-3 samples, but is opposite by applying Freundlich isotherm model, for the same adsorbents.

On the fundamental of the Langmuir analysis, the maximum monolayer sorption capacity (mg/g) q_{max} was calculated and listed in Table 5 for Fe-W-3w and Fe-P-3 nanomaterials. It is noticed that the value of q_{max} was higher for Fe-W-3w than the Fe-P- 3 sample at the same conditions. This may be related to the small agglomeration and particle size of Fe-W-3w adsorbent which facilitates the surface adsorption of dye molecules. Also, this may be attributed

to the regular distribution of porosity as shown in XRD and HR-TEM results. The essential characteristic of the Langmuir isotherm such as the dimensionless separation factor or equilibrium factor (R_L) used in Eq. (11): [14,15,67]

$$R_L = \frac{1}{(1 + K_L C_0)} \tag{11}$$

The R_L refers that isotherm will be shaped according to the following adsorption characteristics: $R_L > 1$ unfavorable; $R_L = 1$ corresponds to linear; $0 < R_L < 1$ is favorable and $R_L = 0$ is irreversible [14,15,67]. According to Table 5, the R_L values were in the range of 0.145–0.189. Therefore, the Langmuir isotherm model is the best to describe the experimental equilibrium data indicating the homogeneous nature of the sample surface and shows the formation of monolayer coverage of dye molecule on the adsorbent external surface.

The isotherm parameters for modeling the experimental results with Freundlich equation are shown in Table 5. $1/n$ values refer to the type of isotherm to be irreversible ($1/n = 0$); favorable ($0 < 1/n < 1$), and unfavorable ($1/n > 1$) [15,67]. As given in Table 5, favorable adsorption of Remazol

Table 5
Adsorption isotherm parameters for adsorption of Remazol red (RB-133) dye onto FeW-3w and Fe-P-3 samples

Samples	Langmuir isotherm model						Freundlich isotherm model					Temkin isotherm model					
	q_{max} (mg/g)	K_L (L/mg)	R^2	R_L	Stand. Error	χ^2	K_F (mg/g)	$1/n$	R^2	Stand. Error	χ^2	α	β	R^2	B (J/mg)	Stand. Error	χ^2
Fe-W-3w	64.103	0.0916	0.978	0.189	0.0202	7.164	10.0424	0.435	0.915	0.456	27.0273	2.670	19.761	0.815	126.674	1.113	61.101
Fe-P-3	48.258	0.1119	0.977	0.145	0.0234	4.559	9.0475	0.397	0.932	0.426	13.0535	1.739	20.656	0.974	121.185	0.209	5.299

red (RB-133) (Reactive dye) onto applied adsorbents can be obtained where $1/n$ values were lower than unity which refers to the favorable uptake of the dyeing process by Freundlich isotherm model. Furthermore, the Freundlich equation produces a minimal fit curve with the experimental data than the Langmuir equation over the whole concentration range examined (Figs. 12a and b).

We can conclude that the Langmuir isotherm model is the best favorable isotherm model to clarify the mechanism of Remazol red (RB-133) adsorption.

The nonlinear form of Temkin relationship can be presented as follows [71]:

$$q_e = \beta \ln(\alpha\, C_e) \tag{12}$$

$$\beta = RT/b$$

where b is the Temkin constant related to the heat of adsorption (J mg^{-1}). q_e is plotted vs. $\ln C_e$ in Fig. 12c, the Temkin constants b, α and β are calculated and the data were recorded in Table 5.

3.5.7. Adsorption thermodynamics

For extra treatise of the effect of temperature on Remazol red (RB-133) dye adsorption, the adsorption thermodynamics was computed. Thermodynamic parameters including the standard free energy change ($\Delta G°$), standard enthalpy change ($\Delta H°$), and standard entropy change ($\Delta S°$)of Remazol red (RB-133) adsorption on the Fe-P-3 sample were calculated at different temperatures 25°C, 35°C and 45°C (298, 308 and 318 K). The values of $\Delta G°$, $\Delta H°$ and $\Delta S°$ were estimated by using the Gibbs free energy equations [72,73]:

$$\Delta G° = -RT \ln K_D \tag{13}$$

$$\ln K_D = \text{constant} - \frac{\Delta H°}{RT} \tag{14}$$

$$\Delta G° = \Delta H° - T\Delta S° \tag{15}$$

where K_D is the variation of the thermodynamic equilibrium constant, which can be calculated from the following relation [74]:

$$K_D = M_w \times 55.5 \times 1{,}000 \times K_L \tag{16}$$

where M_w is the molecular weight of the adsorbate and K_L is the Langmuir constant. The standard enthalpy change is obtained from the slope of the plot between $\ln K_D$ vs. $1/T$, (Fig. not shown, $R^2 > 0.99$). Increasing adsorption of Remazol red (RB-133) with the increase in temperature is supported by determining the enthalpy of adsorption $\Delta H°$ for Remazol red (RB-133) on Fe-P-3 was (24.538 kJ/mol) which is similar to that for the adsorption of RB5 on iron oxide CNPs (24.19 kJ/mol) [3]. A positive standard enthalpy change ($\Delta H°$) proposes that the interaction of Remazol red (RB-133) with the adsorbent is endothermic. While the negative values of ($\Delta G°$) −34.775, −37.964 and −39.711 kJ/mol for Fe-P-3 adsorbent at 25°C, 35°C and 45°C (298, 308 and 318 K), respectively, refer that, the adsorption reaction is more favorable at
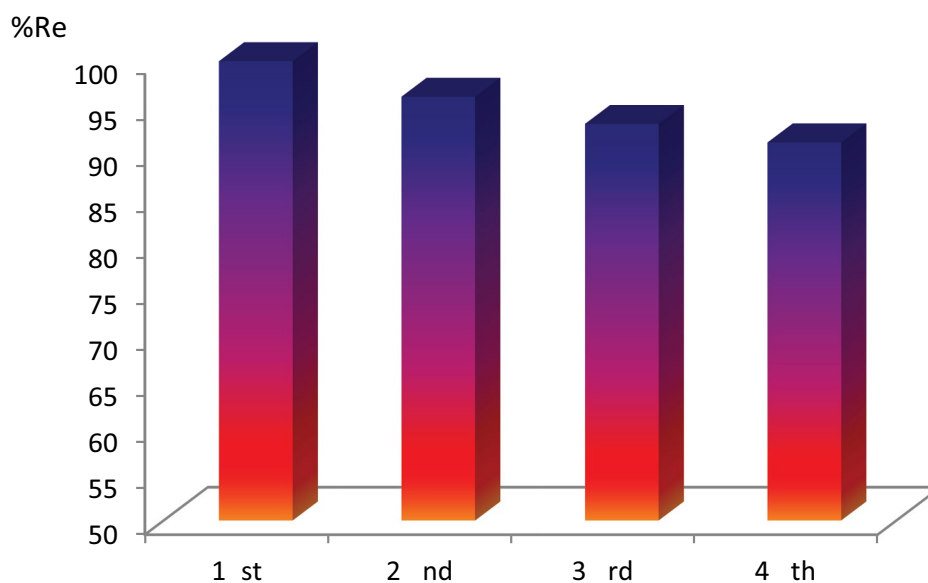
Fig. 13. Remazol Red (RB-133) dye removal percentage by Fe-W-3w adsorbent treated with NaOH solution (dye concentration = 25 ppm, at 25°C and pH = 3).

high temperature and a spontaneous process, as previously reported [3,67]. On the other hand, the positive value of $\Delta S°$ (59.313 kJ/mol K) displayed the increasing of randomness at the solid/solution interface during the sorption of Remazol red (RB-133) on the adsorbent, relating to the growing of the adsorbent surface heterogeneity [3,67].

3.5.8. Desorption and reuse results

Desorption and reuse are important in terms of costs and taking economic feasibility. The Remazol red (RB-133) desorption was possible with NaOH, where, the dye was desorbed in 100 min. These findings emphasize that electrostatic interactions are involved in the dye adsorption. The effectiveness of the used adsorbent treated with NaOH solution, for Remazol red (RB-133) dye removal from aqueous solution was represented by Fig. 13. This figure shows that the as-prepared Fe-W-3w adsorbent can be refreshed by NaOH solution moderately and the reusing was conceivable four times for Remazol red (RB-133), maintaining nearly no change in adsorption capacity; where the removal efficiency still kept 91% even in the fourth cycle. The results referred that Fe-W-3w showed great reusability. Finally, it can be concluded that Fe-W-3w nano-material is an efficient adsorbent in textile Remazol red (RB-133) dye removal whose nature does not change even if it is used for several times.

3.5.9. Adsorption mechanism

The dye removal mechanism by synthesized Hematite (α-Fe$_2$O$_3$) through electrostatic attraction (Fig. 14) was monitored by modifying the solution pH to an acidic condition (pH = 3), so, the surface of the synthesized adsorbent became positive and anionic Remazol red (RB-133) was easily adsorbed. In contrast, the desorption process takes place at higher pH (alkaline medium) which facilitated the desorption process.

Also, it is noticed that forming a colloidal solution with acetic acid and precipitating with water improved the adsorbent capacities. In other words, in the present work Fe-W-3w sample causes high increase in the maximum monolayer sorption ($q_{max} > 64$ mg/g) value compared with previous studies, using magnetic iron oxide nanosphere for Reactive Orange (RO) and Reactive Yellow (RY) removal, q_{max} were 32.5 and 25.0 mg/g, respectively [59]. As mentioned before, this may be attributed to the regular distribution of porosity with applying dispersion–precipitation method by using water into the prepared iron nanomaterial calcined at 300°C, the highest surface area and pore volume coupled with high electrostatic forces of attraction between the adsorbent Fe-W-3w and the textile dye.

4. Conclusion

The main points that have been concluded from the present work are:

- Four different hematite (α-Fe$_2$O$_3$) nanomaterials (Fe-P-T, Fe-W-3w, Fe-W-3d, Fe-A-3) were synthesized by traditional precipitation and dispersion–precipitation method by using acetic acid as a destabilizing agent and the prepared solids calcined at 300°C. Also, certain modifications were applied in the preparation conditions.
- Remazol red (RB-133) dye adsorption from aqueous solution by different prepared hematite (α-Fe$_2$O$_3$) solids has been investigated. The factors that influencing adsorption in the presence of synthesized samples such as preparation conditions, pH of the dye solution, initial dye concentration, time of the attack with dye and adsorption temperature were studied.
- The results showed that Fe-W-3w solid has higher dye uptake rate and adsorption removal 100% than that of the other prepared iron adsorbents in this study or previously reported.
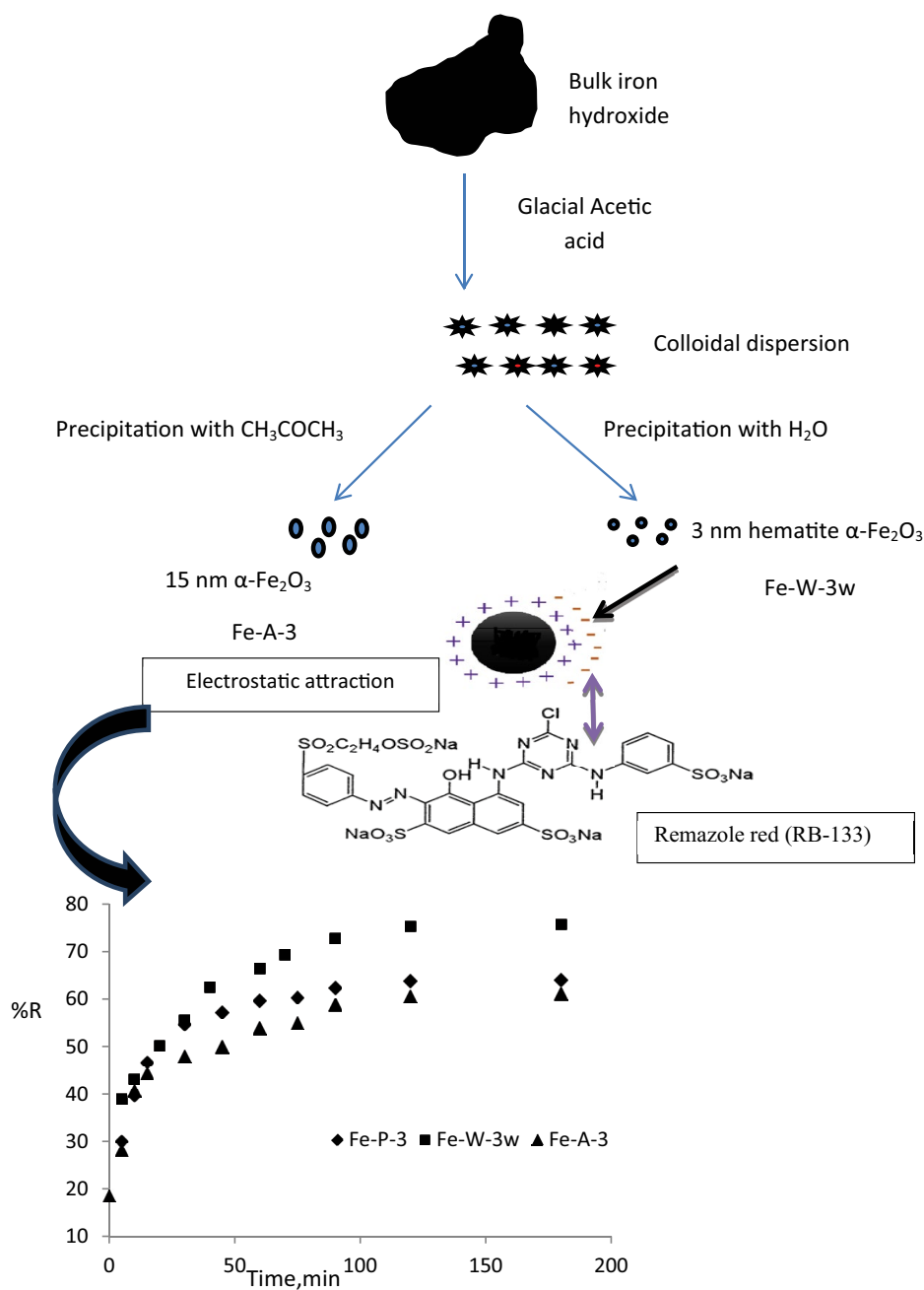
Fig. 14. Removal mechanism of Remazol red (RB-133) by prepared hematite iron oxide adsorbents.

- On the other hand, increasing the pH (>7) or the concentration of the Remazol red (RB-133) dye solution (>50 ppm) decreased the percentage of dye removal from aqueous solutions. Whereas, increasing the time of the attack with dye and/or adsorption temperature led to increasing the % of adsorption removal.
- The adsorption kinetics, thermodynamics and, isotherms were carried out and the results represented that the (PSO) equation and the Langmuir model, respectively, were the best-fitted sorption processes.

- The Fe-W-3w adsorbent can be reused four times for Remazol red (RB-133) dye removal, maintaining the same adsorption capacity. This means that this modified adsorbent is useful in some of the practical applications.
- Finally, the adsorption mechanism of Remazol red (RB-133) dye removing was proposed through high electrostatic forces of attraction between Fe-W-3w solid and the textile dye.

References

[1] K. Isa, D.H. Rezagholipour, A. Mustafa, Preparation, characterization and PE Gylation of superparamagnetic Fe_3O_4 nanoparticles from ethanol medium via cathodic electrochemical deposition (CED) method, Mater. Res. Exp., 3 (2016) 095022.

[2] D. Trpkov, M. Panjan, L. Kopanja, M. Tadić, Hydrothermal synthesis, morphology, magnetic properties and self-assembly of hierarchical α-Fe_2O_3 (hematite) mushroom-, cube- and sphere-like superstructures, Appl. Surf. Sci., 457 (2018) 427–438.

[3] M. Chang, Y. Shih, Synthesis and application of magnetic iron oxide nanoparticles on the removal of Reactive Black 5: Reaction mechanism, temperature and pH effects, J. Environ. Manage., 224 (2018) 235–242.

[4] Y.H. Shih, C.H. Lin, Effect of particle size of titanium dioxide nanoparticle aggregates on the degradation of one azo dye. Environ. Sci. Pollut. Res., 19 (2012) 1652–1658.

[5] H. Gao, R. Cao, X. Xu, J. Xue, S. Zhang,T. Hayat, N.S. Alharbi, J. Li, surface area- and structure-dependent effects of ldh for highly efficient dye removal, Sustain. Chem. Eng., 7 (2019) 905–915.

[6] X. Liu, J. Sun, X. Xu, A. Alsaedi, T. Hayat, J. Li, Adsorption and desorption of U(VI) on different-size graphene oxide, Chem. Eng. J., 360 (2019) 941– 950.

[7] X. Liu, X. Xu, J. Sun, A. Alsaedi, X. Wang, Insight into the impact of interaction between attapulgite and graphene oxide on the adsorption of U(VI), Chem. Eng. J., 343 (2018) 217–224.

[8] S. Duan, X. Xu, X. Liu, Y. Wang, T. Hayat, A. Alsaedi, Y. Meng, J. Li, Highly enhanced adsorption performance of U(VI) by non-thermal plasma modified magnetic Fe_3O_4 nanoparticles, J. Colloid Interface Sci., 513 (2018) 92–103.

[9] E.H.C. Oliveira, D.M.S.M. Fraga, M.P. Silva, T.J.M. Fraga, M.N. Carvalho, E.M.P.L. Freire, M.G. Ghislandi, M.A. Da Motta Sobrinho, Removal of toxic dyes from aqueous solution by adsorption onto highly recyclable xGnP® graphite nanoplatelets, J. Environ. Chem. Eng., 7 (2019) 103001–103010.

[10] T.J.M. Fraga, L.E.M. De Lima, Z.S.B. Souza, M.N. Carvalho, E.M.P.L. Freire, M.G. Ghislandi, M.A. Da Motta, Amino-Fe_3O_4-functionalized graphene oxide as a novel adsorbent of Methylene Blue: kinetics, equilibrium, and recyclability aspects, Environ. Sci. Pollut. Res., 26 (2019) 28593–28602.

[11] S. Sinha, R. Singh, A.K. Chaurasia, S. Nigam, Self-sustainable *Chlorella pyrenoidosa* strain NCIM 2738 based photobio reactor for removal of direct red-31 dye along with other industrial pollutants to improve the water-quality, J. Hazard. Mater., 306 (2016) 386–394.

[12] N.J. Ara, M. Abu Hasan, M.A. Rahman, M. Abdus Salam, A. Salam, A.M.S. Alam, Removal of remazol red from textile waste water using treated sawdust - an effective way of effluent treatment, Bangl. Pharma. J., 16 (2013) 93–98.

[13] M. Ozacar, A. Singel, Adsorption of metal complex dyes from aqueous solutions by pine sawdust, Bioresour. Technol., 96 (2005) 791–795.

[14] H.R. Mahmoud, Sh.M. Ibrahim, S.A. El-Molla, Textile dye removal from aqueous solutions using cheap MgO nanomaterials: adsorption kinetics, isotherm studies and thermodynamics, Adv. Powder Technol., 27 (2016) 223–231.

[15] H.R. Mahmoud, S.A. El-Molla, M. Saif, Improvement of physicochemical properties of Fe_2O_3/MgO nanomaterials by hydrothermal treatment for dye removal from industrial wastewater, Powder Technol., 249 (2013) 225–233.

[16] M.M. Ibrahim, S.A. El-Molla, S.A. Ismail, Influence of γ and ultrasonic irradiations on the physicochemical properties of CeO_2-Fe_2O_3-Al_2O_3 for textile dyes removal applications, J. Mol. Struct., 1158 (2018) 234–244.

[17] S.H. Sajjadia, E.K. Goharshadi, Highly mono dispersed hematite cubes for removal of ionic dyes, J. Environ. Chem. Eng., 5 (2017) 1096–1106.

[18] A. Liu, Z. Xia, W. Zhou, S. Huang, Well-dispersed hematite nanoparticles decorating graphene nanosheets: characterization and performance for methyl orange removal, J. Environ. Chem. Eng., 5 (2017) 6039–6044.

[19] H.A. Eivari, A. Rahdar, Some properties of iron oxide nanoparticles synthesized in different conditions, World Appl. Program., 3 (2013) 52–55.

[20] C.Q. Hu, Z.H. Gao, X.R. Yang, Facile synthesis of single crystalline α-Fe_2O_3 ellipsoidal nanoparticles and its catalytic performance for removal of carbon monoxide, Mater. Chem. Phys., 104 (2007) 429–433.

[21] D.K. Bandgar, S.T. Navale, G.D. Khuspe, S.A. Pawar, R.N. Mulik, V.B. Patil, Novel route for fabrication of nanostructured α-Fe_2O_3 gas sensor, Mater. Sci. Semi cond. Process., 17 (2014) 67–73.

[22] H. Yan, X. Su, C. Yang, J. Wang, C. Niu, Improved photocatalytic and gas sensing properties of α-Fe_2O_3 nanoparticles derived from β-FeOOH nanospindles, Ceram. Int., 40 (2014) 1729–1733.

[23] G. Salek, P. Alphonse, P. Dufour, S. Guillemet-Fritsch, C. Tenailleau, Low-temperature carbon monoxide and propane total oxidation by nanocrystalline cobalt oxides, Appl. Catal., B, 147 (2014) 1–7.

[24] L. Yu, X. Peng, F. Ni, J. Li, D. Wang, Z. Luan, Arsenite removal from aqueous solutions by γ-Fe_2O_3-TiO_2 magnetic nanoparticles through simultaneous photocatalytic oxidation and adsorption, J. Hazard. Mater., 246 (2013) 10–17.

[25] W. Cheng, J. Xu, Y. Wang, F. Wu, X. Xu, J. Li, Dispersion–precipitation synthesis of nanosized magnetic iron oxide for efficient removal of arsenite in water, J. Colloid Interface Sci., 445 (2015) 93–101.

[26] W. Zhang, F. Wu, J. Li, Z. You, Dispersion–precipitation synthesis of highly active nanosized Co_3O_4 for catalytic oxidation of carbon monoxide and propane, Appl. Surf. Sci., 411 (2017) 136–143.

[27] J.J. Li, Z. Mu, X.Y. Xu, H. Tian, M.H. Duan, L.D. Li, Z.P. Hao, S.Z. Qiao, G.Q. Lu, A new and generic preparation method of mesoporous clay composites containing dispersed metal oxide nanoparticles, Microporous Mesoporous Mater., 114 (2018) 214–221.

[28] J.J. Li, R.J. Lu, B.J. Dou, C.Y. Ma, Q.H. Hu, Y. Liang, F. Wu, S.Z. Qiao, Z.P. Hao, Porous graphitized carbon for adsorptive removal of benzene and the electrothermal regeneration, Environ. Sci. Technol., 46 (2012) 12648–12654.

[29] B.D. Cullity, Elements of X-Ray Diffraction, Publishing Cos, 2nd Ed., Addison-Wesley, Reading, MA, United states, 1978.

[30] F. Rouquerol, J. Rouquerol, K. Sing, Adsorption by Powders and Porous Solids: Principles, Methodology and Applications, Academic Press, San Diego, 1999.

[31] A. Lassoued, M.S. Lassoued, B. Dkhil, A. Gadri, S. Ammar, Synthesis, structural, optical and morphological characterization of hematite through the precipitation method: effect of varying the nature of the base, J. Mol. Struct., 1141 (2017) 99–106.

[32] B.d. Rivas, R. López-Fonseca, C. Jiménez-González, J.I. Gutiérrez-Ortiz, Synthesis, characterisation and catalytic performance of nanocrystalline Co_3O_4 for gas-phase chlorinated VOC abatement, J. Catal., 281 (2011) 88–97.

[33] V.A. Drits, J. Srodon, D.D. Eberl, XRD measurement of mean crystallite thickness of illite and illite/smectite; reappraisal of the Kubler index and the Scherrer equation, Clay Clay Miner., 45 (1997) 461–475.

[34] S.E. Karekar, D.V. Pinjari, Sonochemical synthesis and characterization of molybdenum sulphide nanoparticles: effect of calcination temperature, Chem. Eng. Process. Process Intensification, 120 (2017) 268–275.

[35] C. Morterra, A. Chiorlno, E. Borello, An IR spectroscopic characterization of α-FeOOH (goethite), Mater. Chem. Phys., 10 (1984) 119–138.

[36] Z.M. Ristic, S. Music, F. Mossbauer, FT-IR and FE SEM investigation of the formation of hematite and goethite at high pH values, J. Mol. Struct., 141 (2007) 834–836.

[37] H.I. Abdulah, A.M. Farhan, A.J. Ali, Photo-synthesis of nanosized α–Fe_2O_3, J. Chem. Pharma. Res., 7 (2015) 588–591.

[38] R. Barik, M. Mohapatra, Solvent mediated control synthesis of α- Fe_2O_3 with high energy facets oriented mesocrystal for energy storage, Roy. Soc. Chem., 47 (2015) 9203–9215.

[39] B.M. Keyes, L.M. Gedvilas, X. Li, T.J. Coutts, Infrared spectroscopy of polycrystalline ZnO and ZnO:N thin films, J. Cryst. Growth, 281 (2005) 297–302.

[40] H.R. Mahmoud, Novel amorphous mesoporous $0.25Cr_2O_3$-$0.75ZrO_2$ nanomaterials synthesized by a surfactant-assisted hydrothermal method for ethanol oxidation, J. Alloy Compd., 687 (2016) 954–963.

[41] H. Liu, Z. Zhang, X. Wang, G. Nie, J. Zhang, S. Zhang, N. Cao, S. Yan, Y. Long, Highly flexible Fe_2O_3/TiO_2 composite nanofibers for photocatalysis and utraviolet detection, J. Phys. Chem. Solids, 121 (2018) 236–246.

[42] W. Zhang, Z. Ma, L. Du, L. Yang, X. Chen, H. He, Effects of calcination temperature on characterization and photocatalytic activity of $La_2Ti_2O_7$ supported on HZSM-5 zeolite, J. Alloy Compd., 695 (2017) 3541–3546.

[43] J. Li, L. Li, F. Wu, L. Zhang, X. Liu, Dispersion–precipitation synthesis of nanorod Mn_3O_4 with high reducibility and the catalytic complete oxidation of air pollutant, Catal. Commun., 31 (2013) 52–56.

[44] V.D. Mote, J.S. Dargad, B.N. Dole, Effect of Mn doping concentration on structural, morphological and optical studies of ZnO nano-particles, Nanosci. Nanoeng., 1 (2013) 116–122.

[45] L. Ojamäe, C. Aulin, H. Pedersen, P. Käll, IR and quantum-chemical studies of carboxylic acid and glycine adsorption on rutile TiO_2 nanoparticles, J. Colloid Interface Sci., 296 (2006) 71–78.

[46] C.Y. Wang, H. Groenzin, M.J. Shultz, Comparative study of acetic acid, methanol, and water adsorbed on anatase TiO_2 probed by sum frequency generation spectroscopy, J. Am. Chem. Soc., 127 (2005) 9736–9744.

[47] J.J. Li, L. Li, W. Cheng, F. Wu, X.F. Lu, Z.P. Li, Controlled synthesis of diverse manganese oxide-based catalysts for complete oxidation of toluene and carbon monoxide, Chem. Chem. Eng. J., 244 (2014) 59–67.

[48] V.S. Munagapati, D.S. Kim, Adsorption of anionic azo dye Congo Red from aqueous solution by Cationic Modified Orange Peel Powder, J. Mol. Liquids, 220 (2016) 540–548.

[49] P.K. Malik, Use of activated carbons prepared from sawdust and rice-husk for adsorption of acid dyes: a case study of Acid Yellow 36, Dyes Pigm., 56 (2003) 239–249.

[50] T.A. Khan, E.A. Khan, Shahjahan, Removal of basic dyes from aqueous solution by adsorption onto binary iron-manganese oxide coated kaolinite: non-linear isotherm and kinetics modeling, Appl. Clay Sci., 107 (2015) 70–77.

[51] J. Zhang, Q. Zhou, L. Ou, Kinetic, isotherm, and thermodynamic studies of the adsorption of methyl orange from aqueous solution by chitosan/alumina composite, J. Chem. Eng. Data, 67 (2012) 412–419.

[52] C. Jarusiripot, Removal of Reactive Dye by Adsorption over Chemical Pretreatment Coal Based Bottom Ash, Procedia Chem., 9 (2014) 121–130.

[53] J. Liu, Y. Wang, Y. Fang, T. Mwamulima, S. Song, C. Peng, Removal of crystal violet and methylene blue from aqueous solutions using the fly ash-based adsorbent material-supported zero-valent iron, J. Mol. Liquids, 250 (2018) 468–476.

[54] W. Liu, C. Yae, M. Wang, J. Ji, L. Ying, C. Fu, Kinetics and thermodynamics characteristics of cationic yellow X-GL adsorption on attapulgite/rice hull-based activated carbon nanocomposites, Environ. Prog. Sust. Energy, 32 (2012) 655–662.

[55] M. Kosmulski, E. Maczka, E. Jartych,, J.B. Rosenholm, Synthesis and characterisation of goethite and goethite-hematite composite: experimental study and literature survey, Adv. Colloid Interface Sci., 103 (2003) 57–76.

[56] M. Kosmulski, Chemical Properties of Material Surfaces, Marcell Dekker, New York, 2001.

[57] G.V. kumar, M. Dharmendirakumar, S. Renganathan, S. Sivanesan, G. Baskar, K.P. Elango, Removal of congo red from aqueous solutions by Perlite, Clean Soil Air Water, 37 (2009) 355–364.

[58] L. Torkian, B.G. Ashtiani, E. Amereh, N. Mohammadi, Adsorption of congo red on tomesoporous carbon material: equilibrium and kinetic studies, Desal. Wat. Treat., 44 (2012) 118–127.

[59] M. Khosravi, S. Azizian, Adsorption of anionic dyes from aqueous solution by iron oxide nanospheres, J. Ind. Eng. Chem., 20 (2014) 2561–2567.

[60] R. Rahimi, H. Kerdari, M. Rabbani, M. Shafiee, Synthesis, characterization and adsorbing properties of hollow $Zn-Fe_2O_4$ nanospheres on removal of Congo red from aqueous solution, Desalination, 280 (2011) 412–418.

[61] C. Vîrlan, R.G. Ciocârlan, T. Roman, D. Gherca, N. Cornei, A. Pui, Studies on adsorption capacity of cationic dyes on several magnetic nanoparticles, Acta Chem. Iasi, 21 (2013) 19–30.

[62] A. Karamipour, N. Rasouli, M. Movahedi, H. Salavati, A kinetic study on adsorption of Congo Red from aqueous solution by ZnO $ZnFe_2O_4$-polypyrrole magnetic nanocomposite, Phys. Chem. Res., 4 (2016) 291–301.

[63] L.R. Bonetto, F. Ferrarini, C. De Marco, J.S. Crespo, R. Guegan, M. Giovanela, Removal of methyl violet 2B dye from aqueous solution using a magnetic composite as an adsorbent, J. Water Proc. Eng., 6 (2015) 11–20.

[64] Y. Hao, Z. Wang, J. Gou, S. Dong, Highly efficient adsorption and removal of Chrysoidine Y from aqueous solution by magnetic graphene oxide nanocomposite, Arab. J. Chem., (2015) doi: 10.1016/j.arabjc.2015.07.013.

[65] S. Azizian, Kinetic models of sorption: a theoretical analysis, J. Colloid Interface Sci., 276 (2004) 47–52.

[66] Y.S. Ho, G. Makay, A comparison of chemisorption kinetic models applied to pollutant removal on various sorbents, Process Saf. Environ., 76 (1998) 332–340.

[67] N.F. El-Harby, Sh.M. Ibrahim, N.A. Mohamed, Adsorption of Congo red dye onto antimicrobial terephthaloylthio urea cross-linked chitosan hydrogels, Water Sci. Technol.,76 (2017) 2719–2732.

[68] W.J. Weber, J.C. Morris, Kinetics of adsorption on carbon from solution, J. Sanit. Eng. Division, 89 (1963) 31–60.

[69] H. Freundlich, Über die adsorption in lösungen, Z. Phys. Chem., 57 (1906) 385–490.

[70] I. Langmuir, The adsorption of gases on plane surfaces of glass, mica and platinum, J. Am. Chem. Soc., 40 (1918) 1361–1403.

[71] Y. El maataoui, M. El mrabet, A. Maaroufi, H. Oudda, A. Dahchour, Adsorption isotherm modeling of carbendazim and umetsulam onto homoionic-montmorillonite clays: comparison of linear and nonlinear models, Turk. J. Chem., 41 (2017) 514–524.

[72] W.S.W. Ngah, K.H. Liang, Adsorption of Gold (III) Ions onto chitosan and N-carboxymethyl chitosan: equilibrium studies, Ind. Eng. Chem. Res., 38 (1999) 1411–1414.

[73] C. Raymond, Chemistry: Thermodynamic, Von Hoffman Press, Boston, 1998.

[74] H. Tran, S. You, A. Bandegharaei, H. Chao, Mistakes and inconsistencies regarding adsorption of contaminants from aqueous solutions: a critical review, Water Res., 120 (2017) 88–116.